[10] Arlt, H. J., Au, G. F., and Baumgarth, S., "Kaufman Ion Thruster of the DFVLR Braunschweig," The 9th International Aeronautical Congress, Paris, June 1969, AFITAE-preprint, pp. 1–26.

[11] Arlt, H. J., Au, G. F., and Baumgarth, S., "Experimentelle Ergebnisse über das Ionentriebwerk ESKA-18," *Raumfahrtforschung*, Band XIII, Heft 5, Sept./Oct. 1969, pp. 197–204.

[12] Ward, J. W. and King, H. J., "Mercury Hollow Cathode Plasma Bridge Neutralizers," *Journal of Spacecraft and Rockets*, Vol. 5, No. 10, Oct. 1968, pp. 1161–1169.

[13] Csiky, G. A., "Langmuir Probe Measurements in a Discharge from a Hollow Cathode," *Journal of Spacecraft and Rockets*, Vol. 7, No. 4, April 1970, pp. 474–475.

[14] Bahr, A., "Plasmabrückenneutralisator," *Jahresbericht 1968 of the DFL*, pp. 99; also "Hohlkathode," *Jahresbericht 1969 of the DFVLR*, pp. 256–257, DFVLR, Braunschweig, W. Germany.

[15] Flügge, S., "*Handbuch der Physik*," Vol. 22, Springer, Berlin-Göttingen-Heidelberg, 1956, pp. 419–420.

[16] Cooper, D. W. and Kuhns, P. W., "Measurement of Ion and Electron Densities of Electron-Bombardment Ion-Thruster Beam," TN D-3761, Dec. 1966, NASA.

[17] Freisinger, J. and Löb, H. W., "Auslegungsgrößen von HF-Triebwerken bei Raumtests," DGLR-Symposium Raumfahrtantriebe II, March 22, 1969, Hannover, Germany.

APRIL 1971 J. SPACECRAFT VOL. 8, NO. 4

A Photographic and Analytic Study of Composite Propellant Combustion in an Acceleration Field

P. G. WILLOUGHBY,* C. T. CROWE,† AND K. L. BAKER‡
United Technology Center, Sunnyvale, Calif.

The experimental fact that acceleration of a composite propellant can effect a significant augmentation of the burning rate is well known. However, an adequate physical insight of the responsible phenomena has been lacking. This paper reports the results of photographing a burning metalized composite propellant under acceleration. The photographic details reveal the inertial retention of burning aluminum particles and the subsequent formation and growth of pits in the surface. An analytic model is developed based on the buoyancy of the globule by combustion gases flowing from the pit bottom and the attendant increased heat transfer from the hot particle, through the supporting gas flow to the propellant surface. The model adequately explains the observed trends in acceleration-produced burning-rate augmentation with ballistic and propellant parameters.

Nomenclature

c_s = specific heat of propellant
e = eccentricity
h_v = heat of vaporization
H_v = $c_s(T_s - T_\infty) + h_v$
n = burning rate exponent
P = pressure
Pe,Pr = Peclet and Prandtl numbers, respectively
Q = heat transfer rate
r,r_s = radial coordinate and globule radius, respectively
$\dot{r}$ = burning rate
Re = Reynolds number
T = temperature
v = velocity
w = metal loading
α = acceleration
η = radial distance along the surface
θ = slope of pit wall
λ = separation distance
μ = gas viscosity
φ = angle between acceleration vector and the normal to the propellant surface
ρ = density
σ = surface tension

Subscripts

a = acceleration
c = chamber
e = edge
f = flame
g = gas
∞ = initial
o = static, surface
p = particle
r = radiation
s = surface, propellant
z = normal coordinate

Presented as Paper 69-173 at the AIAA 7th Aerospace Sciences Meeting, New York, January 20–22, 1969; submitted February 19, 1969; revision received August 6, 1970. This study was performed under contract with the Naval Ordnance Systems Command, Contract N00017-67-C-2429. The technical effort was supported and monitored by B. Drimmer. The photographic work was assisted by D. Girroir. L. Mahle, as well as other members of the Physical Sciences Laboratory, ably assisted in the technical effort. The authors wish to extend their appreciation to these people.

* Senior Scientist, Physical Sciences Laboratory.

† Senior Staff Scientist, Physical Sciences Laboratory now Associate Professor, Washington State University.

‡ Senior Scientist, Physical Sciences Laboratory; now with Electro Optics Associates.

Introduction

IT has long been known that spinning an internal-burning solid-propellant rocket motor about its longitudinal axis for directional stability can significantly affect the motor's internal ballistics. Usually the propellant burning rate and attendant chamber pressures are higher than they would be in the identical motor fired under no-spin conditions.[1] The centrifugal acceleration field is undoubtedly responsible for the augmented regression rate, but understanding of the interaction has been lacking. In order to gain some appre-

ciation of the physical processes involved, an experiment was developed to photograph the burning surface of an accelerated propellant, and an analytical model of the phenomenon was developed.

Photographic Study

The apparatus (Fig. 1) comprised a 24-in.-diam aluminum table rotated by a 1-hp electric motor through a variable-speed hydraulic transmission, producing accelerations up to 900-g at the radius of the propellant sample. An electrical slip-ring assembly conducted power to the photographic light source, shutter, propellant ignitor, and purge solenoid valve. Four-high-pressure bottles, a pressure regulator and solenoid valve were mounted on the table to provide purge gas for the combustion bomb. A multichannel cam timer sequenced the operations.

The combustion bomb was similar to that used by Crump.[2] A $\frac{1}{4}$-in.-square propellant sample, inhibited on three sides with plexiglass applied in a chloroform solution, was mounted on a platform at the center of the bomb. A continuous flow of nitrogen at 2 fps past the sample prevented accumulation with of smoke in the optical path. The propellant was ignited a hot wire in conjunction with a nitrocellulose glue and boron potassium nitrate powder. A pressure transducer measures the combustion pressure. The bomb was connected by $\frac{3}{8}$-in. stainless steel tubing to a similar tank which provided a pressure ballast as well as dynamic balance. This tank contained a blowout disk, which ruptured when the desired pressure was reached, and an orifice to regulate the velocity of the purge gases.

Three series of experiments were conducted at 280 psi with propellant[3] which contains 16% aluminum, 68% ammonium perchlorate, and 16% polybutylene acrylic acid acrylo nitrite (PBAN) binder. The mass-median diameter of the aluminum powder is 47 μ and the ammonium perchlorate had a bimodel distribution 68%, 400 μ and 32%, 7 μ powder. The burning rate at 1000 psi is 0.24 in./sec.

A Photosonic 16-mm motion picture camera was used to photograph the burning propellant. The image was projected through a 135-mm lens (Nikkor-Q Auto 1:3.5) and mirror system to the camera mounted above the table. Although the projected image rotated with respect to the camera, this was no handicap for frame-by-frame analysis. In the first test series a General Electric Marc 300/16 arc lamp with a dichoric reflector, and filtered to restrict the incident radiation to the usable visible light, illuminated the sample. This lamp's measured radiant flux of 2–3 cal/cm^2/sec was sufficient for color photography up to 4000 frames/sec. The hot mirror IR interference filter cracked during testing but continued to reflect the IR radiation. In test series 2 and 3, the light emitted from the burning aluminum particles was the only illumination used (at f22). Either Kodak EF (Daylight) or EFB (Tungsten) color film was used. The magnifications were 1, 2, and $\frac{1}{2}$, in test series 1, 2, and 3, respectively. In each series accelerations of 0, 25 (300 rpm), and 50 g normal and toward the burning surface were run. The camera was focused on the uninhibited front surface, $\frac{1}{16}$ in. behind the front surface and at the center of the propellant sample.

Experimental Results

In the movies the main interest centered around the activity of the burning aluminum particles on the propellant surface. The photographs of the nonaccelerated propellants reveal the same phenomena reported by Crump.[2] Aluminum particles emerge, agglomerate, coalesce upon ignition and continue to burn as they are carried away by the exhaust gases. They have long bright tails, indicating at least partial metal combustion by the vapor diffusion mechanism. In the experiments conducted under acceleration the burning aluminum particles were observed moving about the surface, some colliding and coalescing, while others moved to the edge of the strand and fell off.

The sizes of the burning particles on the burning surface under static and acceleration conditions were measured. Care was exercised in selecting particles that had not undergone collisions on the burning surface. A mass median diameter of about 220 μ was measured for both static and acceleration conditions, indicating that acceleration does not significantly influence particle size. This value agrees with the predicted value for this particular propellant formulation.[3]

In the static experiments the burning surface regressed uniformly, whereas it became very irregular during the acceleration experiments. Even though the history of a given pit could not be followed due to the restricted focal volume, the burning aluminum particles were observed moving downward along the inclined pit walls to areas of very intense local combustion. During each of these experiments a large incandescent particle could be seen on the strand mounting post as the propellant burned out. Postfire examination of these particles showed they have a porous structure very similar to the slag globules found on the grain cases of the spinning motors. At the 50-g level the retention of the burning aluminum agglomerates and the formation of pits on the propellant surface was much more pronounced than at the 25-g level.

The results of the experiments at a magnification of 2 indicated that the framing rate of 1000 pictures/sec was insufficient to give the time resolution necessary for detailed observation of phenomena occurring on the burning surface. However, during the 50-g experiment a pit formed near the front surface of the sample and a large burning agglomerate came into sharp focus. This allowed detailed observation of the burning agglomerate as well as phenomena occurring at the pit walls; three successive frames are shown in Fig. 2. The large 870-μ particle is seen burning in the bottom of a well developed pit. An adjacent pit is evident in the upper left corner. A number of 100–300 μ agglomerates are also

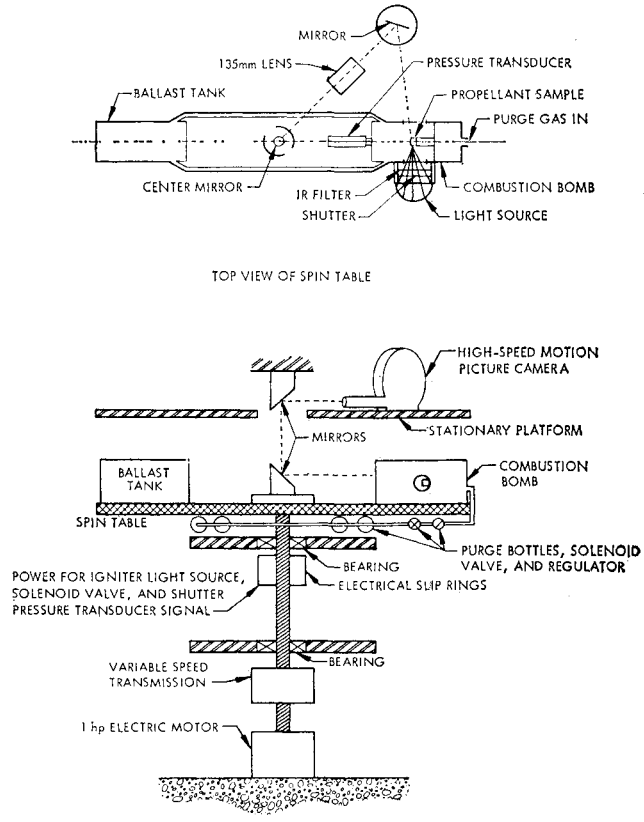

Fig. 1 Schematic diagram of experimental apparatus for photographic combustion studies.

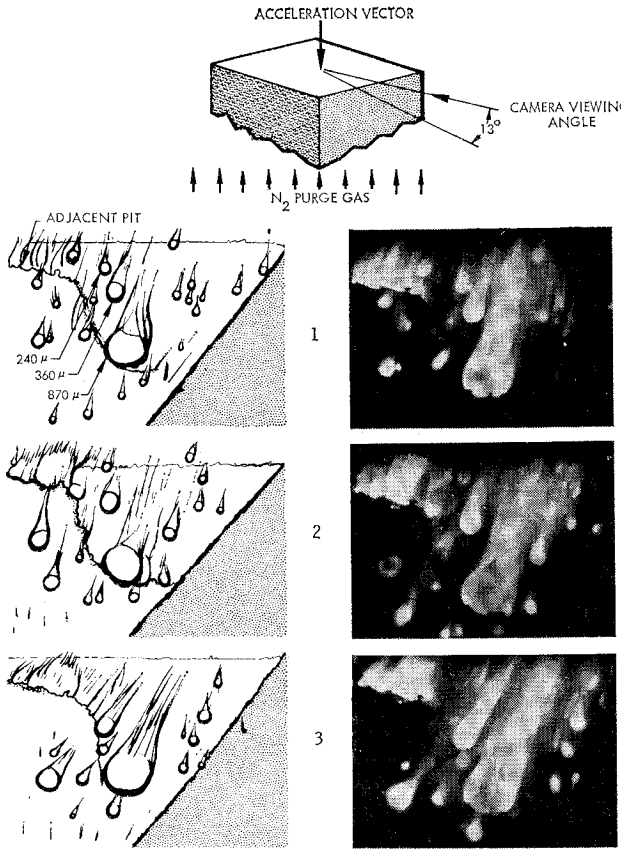

Fig. 2 Photographs and schematic drawing of aluminized propellant combustion under acceleration.

noted burning on or near the propellant surface. All of the particles have bright tails characteristic of the submicron vapor phase metal combustion products. This series of frames illustrates a mechanism of particle growth once a pit has formed. In frame 1 three particles are emerging from the pit wall above and to the right of the large agglomerates. In frame 2 they have coalesced and ignited, and the agglomerate is proceeding down the pit wall. In frame 3 the particle has impinged on, and is burning on the large particle in the pit bottom. The agglomeration process of frames 1 and 2 is seen under static as well as acceleration conditions. The phenomena of impingment and combustion are seen repeatedly in the movies. Another striking feature of the photographs is the uniform character of the flow about the burning particles. This lends support to the theoretical model presented below.

In the series of experiments with a magnification equal to $\frac{1}{2}$ the entire burning surface could be brought into focus. In the 25-g experiment the aluminum agglomerates "danced" about the surface until two or more would collide. The new larger particle would remain stationary, and a pit would develop. At 50 g the dancing particles appeared restrained, and surface pitting occurred earlier. Considering the balance between the opposing centrifugal and aerodynamic drag forces provides some insight into this behavior. These forces are approximately equal for a 200-μ particle subjected to 25-g acceleration burning on the control propellant at 280 psia. If either the particle size or acceleration level is increased, the centrifugal force dominates, and the burning particle is retained on the burning surface.

Review of Observed Effects and Development of Model

It was originally postulated[3] that the augmented burning rate is the result of inertial forces retaining burning metal particles on the propellant surface and thereby increasing the heat transfer rate into the propellant. An analysis was developed in which it was assumed that metal particles are retained on the surface until they become small enough to be transported away by the combustion gases; the heat generated by particle combustion during this time was related to the augmented burning rate. However, this simple model did not adequately explain various effects of propellant and ballistic parameters. The model was extended and improved by Glick,[4] who proposed that the burning metal particles are held by inertial forces at the botton of pits in the propellant surface. This concept was stimulated by the discovery[5] that the entire surface of a prematurely-extinguished accelerated propellant is pitted. He assumed that the particle burning rate is just sufficient to consume the metal powder which emerges from the regressing pit walls and falls on the particle at the pit bottom. The heat liberated by particle combustion is assumed responsible for a locally augmented burning rate at the pit bottom. This improved model still was inadequate to explain various trends. A seemingly more promising approach results from a detailed study of the flow character between the retained particle and propellant surface, as we shall discuss after reviewing the various experimental observations on acceleration-produced burning-rate augmentation.

Observed Effects

Fundamental data have been obtained using two testing techniques: spinning internal-burning motors[1] and burning propellant on a centrifuge.[5–7] The burning-rate augmentation $\dot{r}_a/\dot{r}_o$ is defined as the measured burning rate under acceleration normalized with respect to the burning rate which would exist at static conditions at the same pressure level. The following paragraphs discuss the parameters which affect $\dot{r}_a/\dot{r}_o$ for composite propellants.

Magnitude and direction of acceleration vector. For many propellants there appears to be a threshold acceleration,[3] below which little effect is noted, and above which $\dot{r}_a/\dot{r}_o$ increases rapidly and then tends toward a maximum value with increasing acceleration normal toward the burning surface. The burning rate is unchanged[7] by acceleration parallel to the burning surface or by acceleration directed away from the propellant surface.[5] Northam and Lucy[8] have found that, in the acceleration regime of their experiments, the burning rate returned to very near the static value when the acceleration vector was inclined at more than 15° from the normal to the surface.

Pressure level. The effect of P_c appears to vary with propellant type and pressure level. Northam, using an aluminized polybutadiene acrylic acid (PBAA) propellant, measured burning rates at accelerations up to 300 g and at pressures between 300 and 1000 psi. His data show that large changes in pressure do not cause large changes in $\dot{r}_a/\dot{r}_o$. Anderson, using a similar propellant in his strand burner experiments, found an appreciable decrease in $\dot{r}_a/\dot{r}_o$ as P_c was increased to 1500 psi, and he reported an inordinate amount of alumina residue at high P_c; UTC has observed the same phenomena. For polyurethane propellants at 200 g, however, Lucy§ reports that $\dot{r}_a/\dot{r}_o$ is quite sensitive to P_c, increasing by 25% as P_c is raised from 250 to 1000 psi, and increasing further as P_c is raised further. It is important to note that this propellant under static conditions had a burning-rate exponent of 0.06.

Static burning rate, r_o. The most important parameter controlling $\dot{r}_a/\dot{r}_o$, save acceleration itself, is $\dot{r}_o$. Burning-rate data for low-$\dot{r}_o$ polyurethane propellants show $\dot{r}_a/\dot{r}_o > 3$,[8] whereas data[9] for high-$\dot{r}_o$ propellants show no measurable effect of acceleration at the same acceleration levels. A definitive experiment on the significance of $\dot{r}_o$ has been performed by UTC. A conventional propellant formulation containing

§ Private communication.

16% aluminum, with $\dot{r}_o = 0.16$ in./sec at 500 psi, showed $\dot{r}_a/\dot{r}_o = 3.1$ at 500 g. A burning-rate catalyst was added to the same formulation to increase $\dot{r}_o$ by a factor of two; then $\dot{r}_a/\dot{r}_o$ was only 1.3 at 500 g.

Metal content and powder size. Several experiments have shown that for nonmetalized polybutadiene propellants, there is no appreciable increase in $\dot{r}$ below 100-g acceleration and then an increase toward a nominal value of 1.3 as the acceleration is further increased. Sturm[10] has proposed that the burning-rate augmentation of nonmetalized propellants is due to the retention of oxidizer particles on the surface. Glick has suggested the effect of acceleration on the transport of "fuel vapor pockets" as the responsible mechanism. The experimental verification of either model is still lacking.

The inclusion of metal in the propellant produces various effects. The experiments of UTC indicate that increasing the metal content increases $\dot{r}_a/\dot{r}_o$ at acceleration levels below 100 g. Anderson observed the same trend. However, at accelerations >200 g, Anderson's data reveal that $\dot{r}_a/\dot{r}_o$ is reduced as the metal content is increased. The same trend has been observed by Northam and Lucy.

Tests by UTC and others have shown that $\dot{r}_a/\dot{r}_o$ is reduced by utilizing finer powder.

Experiments which have provided significant insight into the mechanisms which control burning-rate augmentation are those in which a refractory was substituted for the combustible metal. Experiments were performed by UTC in which tungsten and alumina (Al_2O_3) were used in place of aluminum, and $\dot{r}_a/\dot{r}_o$ was significantly increased, especially with the tungsten additive. Postfire inspection of the motors revealed no residue from the tungsten propellant, while the liner of the expended alumina-propellant was covered by a continuous layer of Al_2O_3. Sturm also found higher $\dot{r}_a/\dot{r}_o$ for propellants with an alumina additive. The unlikelihood of refractory combustion sheds doubt on the validity of any physical model based solely on augmented burning rate by heat release due to particle combustion alone.

Burning time. Sturm, in his experiments with strands of varying length,[10] discovered that the $\dot{r}_a/\dot{r}_o$ decreased with increasing strand length (increasing burning time). UTC has noticed with its spinning-motor tests that burning rate first increases, reaches a maximum and decreases toward a stable value. However, it was impossible to determine from these tests whether this effect was a real transient burning rate phenomenon or the result of slagging at the nozzle throat.

Development of Physical Model

Postfire inspection of motor cases from spinning-motor tests show discrete platelets of aluminum oxide adhering to the propellant liner. The platelet surface-density appears to conform closely to the pit density determined from premature extinguishment tests. It is thereby postulated that each platelet is the particle that was centrifugally held at the bottom of a pit, and that the particle, or globule (as we shall call it hereafter) is buoyed above the pit bottom by the combustion gases (Fig. 3) and is maintained at a temperature close to the chamber temperature. The heat transferred across the gas layer to the propellant surface is assumed responsible for the augmented burning rate. The validity of this model gains considerable support from the successful cinematography of a burning propellant surface under acceleration reported in the previous section. These photographs clearly show the existence of hot condensed-phase globules which create persisting pits owing to the locally increased burning rate beneath the globule.

In Fig. 3, the liquid alumina globule, flatted by inertial forces, is retained at the bottom of a pit where the local burning rate is $\dot{r}_a$. If one assumes that the pit wall regresses at the static rate, its slope is given by

$$\theta = \cos^{-1}(\dot{r}_o/\dot{r}_a) \tag{1}$$

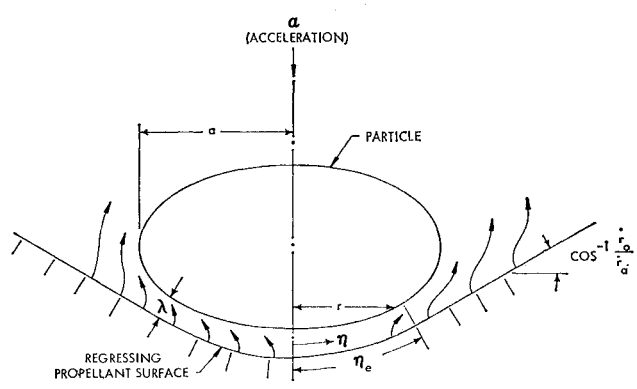

Fig. 3 Proposed physical model.

The combustion gases flowing out from beneath the globule effect an increased pressure on the under surface which balances the globule's inertial force. Order-of-magnitude calculations[9] indicate that the effect of the increased pressure alone is insufficient to account for the augmented burning rate. It can be shown that the radiative heat transfer from the hot globule is also unable to explain the augmented burning rates. Thus one is led to consider conductive heat transfer as the responsible mechanism.

An approximate analysis is first necessary to assess the character of the flow beneath the globule. Assume, for purpose of analysis, that the globule is spherical and the distance between the globule and surface sufficiently small so that the flow may be regarded as that between two parallel surfaces. The continuity equations for this cylindrically symmetric flow, neglecting for now the presence of the nongasifiable metal additives, is

$$\lambda d(\rho\eta v_g)/d\eta = \eta\dot{r}_a\rho_s \tag{2}$$

where ρ_g = gas density, λ = separation distance, η = radial distance along the surface, v_g = gas velocity, and ρ_s = propellant density. Integrating this expression yields the radial mass flux

$$\rho_g v_g = \dot{r}_a\rho_s\eta/2\lambda \tag{3}$$

The corresponding momentum equation, neglecting for now the viscous forces, is

$$(1/\eta)(d/d\eta)(\rho_g v_g{}^2\eta) = -dP/d\eta \tag{4}$$

Assuming that ρ_g is independent of η and that the pressure P decays to the chamber pressure P_c at the globule's edge, η_e, gives

$$P(\eta) = (1/\rho_g)(\rho_s\dot{r}_a/2\lambda)^{\frac{3}{2}}(\eta_e{}^2 - \eta^2) + P_c \tag{5}$$

Globule buoyance requires a balance of inertial and pressure forces, or

$$\tfrac{4}{3}\pi r_s{}^3\rho_p\alpha = 2\pi\int_0^r \Delta P r dr \tag{6}$$

where ρ_p = globule density, α = acceleration, r_s = globule radius, r = radial coordinate, and $r_e = r$ at the globule edge. Assuming the locus of the globule's edge is its equator and integrating Eq. (6) using $\Delta P = P(\eta) - P_c$ from Eq. (5) yields the normalized separation distance

$$\lambda/r_s = 0.7(\rho_s\dot{r}_a)/(\rho_p\rho_g\alpha r_s)^{1/2} \tag{7}$$

Substituting typical values for these parameters, such as $\dot{r}_a = 1$ cm/sec, $\rho_s = 1.8$ g/cm^3, $\rho_p = 4$ g/cm^3, $\rho_g = 3 \times 10^{-3}$ g/cm^3, 100 g, and $r_s = 250$ μ shows that $\lambda/r_s = \mathcal{O}(0.1)$. Thus, the analysis of the flow assuming parallel boundaries is sufficiently valid.

The characteristic Reynolds number of the flow is

$$Re = \rho_s\dot{r}_a\lambda/\mu \tag{8}$$

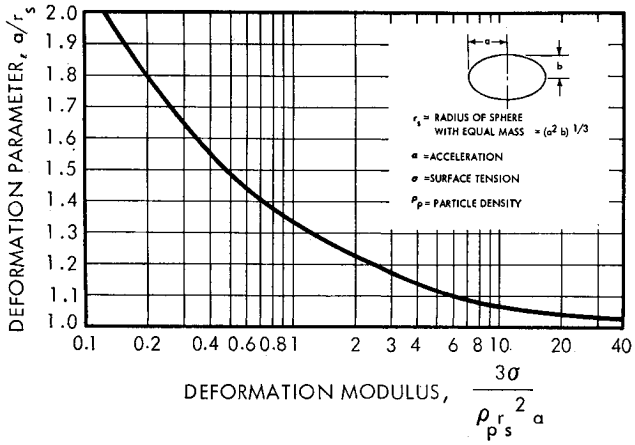

Fig. 4 Deformation of an oblate spheroid in an acceleration field.

where μ is the gas viscosity. Taking a reasonable value of 7×10^{-4} poise for μ and using the above parameters give $Re = \mathcal{O}(10)$, which indicates the flow should be laminar.

It can also be easily shown that the Mach number of the gases is $\mathcal{O}(0.1)$. Because the Mach number is low, compressibility effects are unimportant. But there will be a density variation because of the temperature difference between the surface and the globule. For the present purposes, however, a constant density flow is analyzed to provide the essential parametric relationships and avoid the more cumbersome approach. The results for the pressure distribution and surface enthalpy gradient are presented in the Appendix.

A significant feature of the analysis is the effect of acceleration on globule shape. Because the alumina globule must be at a temperature near the rocket chamber temperature (3300°K), it must be in the liquid state. Several analyses exist for the shape of a liquid droplet which rests on a flat surface. However, they are not applicable in this situation because the alumina globule does not rest on, nor wet, the propellant surface.

A reasonable approach is to assume the globule shape is an oblate spheroid. As the eccentricity of a constant-volume globule is varied, there is a change in potential energies associated with surface tension forces and displacement of the center-of-mass in the centrifugal force field. At the point of stable equilibrium, the change in total energy with a small perturbation in eccentricity is zero. Performing this analysis[9] yields the curve shown in Fig. 4 for a/r_s vs $3\ \sigma/\rho_p r_s^2 \alpha$, where a is the particle's major radius, r_s its equivalent-sphere radius, and σ its surface tension. This relationship can now be used to estimate the particle shape under the various conditions.

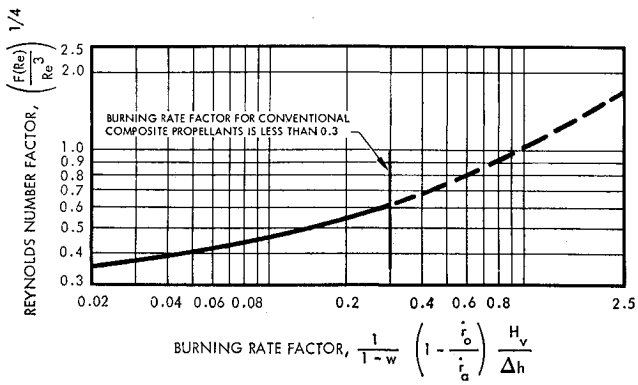

Fig. 5 Reynolds number factor vs burning rate factor as derived from energy balance at burning surface.

The globule-surface separation distance is established by equating the pressure and inertial forces. The pressure distribution beneath the globule, derived in the Appendix, is

$$P = P_c + (\rho_g v_{zo}^2/\lambda^2)(3/Re)F(Re)(\eta_e^2 - \eta^2) \qquad (9)$$

where v_{zo} the normal gas velocity at the surface, and

$$F(Re) = (1 + Re/2 + Re^2/6 + Re^3/24)/(1 + Re/2 + 3Re^2/20)$$

and Reynolds number is defined as $Re = \rho_g v_{zo}\lambda/\mu$. The globule edge η_e is defined as that point where P reduces to P_c, and it is assumed that the slope of the particle surface departs from that of the propellant surface at η_e (see Fig. 3). Using Eq. (9) and equating the pressure and inertial forces yields

$$\frac{2}{9}\rho_p r_s^3 \alpha = \frac{\mu^2}{\rho_g}\left(\frac{a}{\lambda}\right)^4 Re\,F(Re)\int_0^{\bar{\eta}_e}(\bar{\eta}_e^2 - \bar{\eta}^2)\bar{r}\,d\bar{r} \qquad (10)$$

where the bar represents nondimensionalization with respect to the globule's major radius. Introducing the following expression for the normal gas velocity at the surface

$$v_{zo} = \rho_s \dot{r}_a/\rho_g(1 - w) \qquad (11)$$

where w is the weight fraction of metal in the propellant, Eq. (10) becomes

$$\left(\frac{2}{9}\right)^{1/4}\frac{r_s}{a}\left(\frac{\rho_p \rho_g \alpha}{r_s}\right)^{1/4}\frac{\mu^{1/2}}{\rho_s \dot{r}_o(1 - w)} = \left(\frac{\dot{r}_a}{\dot{r}_o}\right)\left[\frac{F(Re)}{Re^3}\right]^{1/4} \times \left[\int_0^{\bar{\eta}_e}(\bar{\eta}_e^2 - \bar{\eta}^2)\bar{r}\,d\bar{r}\right]^{1/4} \qquad (12)$$

The integral factor is a function of the globule's eccentricity and value of the edge coordinate.

An additional equation is now needed to associate the augmented burning rate and globule-surface separation distance. This is obtained through relating the augmented burning rate and the heat transfer to the surface. The heat transfer balance at the propellant surface is given by

$$c_s \rho_s \dot{r}(T_s - T_\infty) + h_v \rho_s \dot{r} = \dot{Q}_f + \dot{Q}_s + \dot{Q}_r \qquad (13)$$

where c_s is the specific heat of the propellant, T_s the surface temperature, T_∞ the initial propellant temperature, h_v the heat of vaporization, $\dot{Q}_f$ the heat-transfer rate from the flame by conduction, $\dot{Q}_s$ heat produced by surface reactions, and $\dot{Q}_r$ heat transfer rate due to radiation. Assuming that the presence of the globule does not appreciably influence T_s, $\dot{Q}_s$, and Q_r, one concludes

$$\dot{Q}_{fa} - \dot{Q}_{fo} = \rho_s(\dot{r}_a - \dot{r}_o)H_v \qquad (14)$$

where $H_v = c_s(T_s - T_\infty) + h_v$ and the subscripts a and o refer to acceleration and static conditions, respectively. It is assumed that the increased heat transfer rate due to conduction is that conducted from the hot globule to the surface, or

$$\dot{Q}_{fa} - \dot{Q}_{fo} = (\mu/Pr)\partial h/\partial z = \rho_s(\dot{r}_a - \dot{r}_o)H_v \qquad (15)$$

where Pr is the Prandtl number and h the specific enthalpy of the gases, respectively. Using the expression for the enthalpy gradient derived in the Appendix yields

$$\frac{Pe^{1/2}}{1 - w}\left(1 - \frac{\dot{r}_o}{\dot{r}_a}\right)\frac{H_v}{\Delta h} = \left(\frac{2}{\pi}\right)^{1/2}\frac{\exp(-Pe/2)}{\operatorname{erf}(Pe/2)^{1/2}} \qquad (16)$$

where Pe is the Péclet number.

The variation of the factor $[F(Re)\cdot Re^{-3}]^{1/4}$ with $(1 - \dot{r}_o/\dot{r}_a)(H_v/\Delta h)/(1 - w)$ as determined by Eq. (16) is illustrated in Fig. 5. A typical value of 0.75 was assumed for the Prandtl number. A reasonable estimate of Δh can be achieved by assuming a globule temperature of 3300°K, a surface temperature of 900°K, and an average specific heat of the gases of 0.4 cal/g°K. Then $\Delta h \simeq 1000$ cal/g.

Reference to the literature suggests that a reasonable value for H_v is 250 cal/g. It is evident that the abscissa cannot exceed $(H_v/\Delta h)/(1 - w)$ which, for the previously mentioned values, is about 0.3. In the region of interest it is noted that $[F(Re)\cdot Re^{-3}]^{1/4}$ is not a strong function of $(1 - r_o)/(r_a)(H_v/\Delta h)/(1 - w)$ and it is permissible to neglect the effect of the metal loading on the Reynolds number factor.

Using the aforementioned relationships for $[F(Re)\cdot Re^{-3}]^{1/4}$ as a function of $\dot{r}_o/\dot{r}_a$ and evaluating the integral in Eq. (12) as a function of burning-rate augmentation and particle eccentricity e, provides the following relation

$$\left(\frac{2}{9}\right)^{1/4}\frac{r_s}{a}\left(\frac{\rho_p\rho_g\alpha}{r_s}\right)^{1/4}\frac{\mu^{1/2}K}{\rho_s\dot{r}_o(1 - w)} = A\left(\frac{\dot{r}_o}{\dot{r}_a},e\right) \qquad (17)$$

where $A(\dot{r}_o/\dot{r}_a,e)$ is the augmentation function shown in Fig. 6, and K is an empirical constant to account for lack of knowledge of such parameters as heat of vaporization, viscosity, and others. One notes that $A(\dot{r}_o/\dot{r}_a,e)$ is not a strong function of eccentricity.

Let us evaluate the order of magnitude of the burning rates predicted using reasonable values for the parameters in Eq. (17). Northam's sieve analysis of alumina globules retained on the burner slab after burnout of a 100-g test indicated diameters of the order of 800 μ. Assuming a surface tension of 600 dynes/cm for molten aluminum oxide and using Fig. 4 predicts $a/r_s \simeq 1.15$, which corresponds to an eccentricity of 0.7. The other parameters which characterize the experimental conditions are

$\rho_g = 2.5 \times 10^{-3}$ g/cm^3	$\rho_s = 1.8$ g/cm^3
$\rho = 3.8$ g/cm^3	$\dot{r}_o = 0.74$ cm/sec
$\mu = 7 \times 10^{-4}$ poise	$w = 0.16$

Substituting these values into Eq. (17) and taking $K = 1$ yields $A(\dot{r}_a/\dot{r}_o, e) = 0.18$. Reference to Fig. 6 predicts $\dot{r}_a/\dot{r}_o = 1.13$, which agrees closely with the value of 1.16 measured by Northam. This calculation demonstrates that the proposed model is reasonable in that the heat transfer rate from the globules to the surface is of the order of magnitude sufficient to cause the observed burning-rate increases.

Discussion of Physical Model

The ultimate test of the physical model is its ability to explain observed trends. For purposes of this study, the following approximation for the augmentation function

$$A(\dot{r}_a/\dot{r}_o,e) \simeq \tfrac{1}{5} + \tfrac{1}{2}(\dot{r}_a/\dot{r}_o - 1) \qquad (18)$$

is acceptable for $\dot{r}_a/\dot{r}_o > 1.2$. Thus, we can write

$$\dot{r}_a/\dot{r}_o = 2[(r_s/a)(\rho_p\rho_g\alpha/r_s)^{1/4}\{k/\rho_s\dot{r}_o(1 - w)\} - 0.2] + 1 \qquad (19)$$

for $\dot{r}_a/\dot{r}_o > 1.2$. The significance of each parameter will be discussed in turn.

Magnitude and orientation of acceleration vector. The analysis implies that $\dot{r}_a/\dot{r}_o$ varies as the $\frac{1}{4}$th power of α. This trend corresponds to the observed rapid increase in $\dot{r}_a/\dot{r}_o$ at low α's and a leveling-off toward higher α's. Of course, a more detailed study would include the effect of α on particle size and shape. The model is inadequate to predict the dependence of $\dot{r}_a/\dot{r}_o$ on ϕ, the angle between the acceleration vector and the normal to the propellant surface. However, knowledge of $\dot{r}_a$ provides a limiting condition. In order for a pit to exist, the component of $\dot{r}_a$ normal to the pit wall must exceed $\dot{r}_o$, or $\phi < \cos^{-1}(\dot{r}_a/\dot{r}_o)$. Northam and Lucy tested a propellant at an α for which $\dot{r}_a/\dot{r}_o \simeq 1.2$ (at $\phi = 0$) and found that $\dot{r}_a/\dot{r}_o \to 1$ at $\phi \simeq 15°$. The foregoing inequality predicts that $\phi < 33°$, which agrees qualitatively with the experimental observations.

Pressure level. If $\rho_g \sim P_c$, and $\dot{r}_o$ obeys Vielle's law, Eq. (19) yields the approximate result $\dot{r}_a/\dot{r}_o \alpha P_c^{1/4-n}$ which implies that for conventional propellants, which have a burning-rate

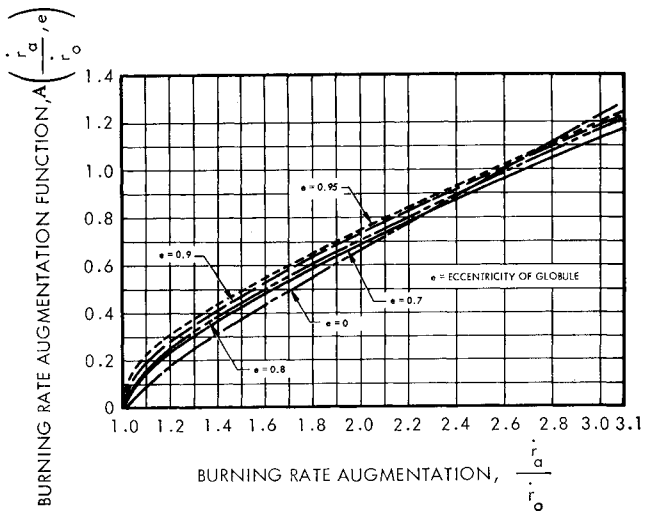

Fig. 6 Burning-rate augmentation function vs burning-rate ratio.

exponent n near 0.25, $\dot{r}_a/\dot{r}_o$ is not significantly affected by pressure level. This, in principle, agrees with Northam's results. For the polyurethane propellants investigated by Lucy, $n \simeq 0.06$, which, from the preceding expression, suggests $\dot{r}_a/\dot{r}_o \sim P_c^{0.19}$. Raising P_c from 250 to 1000 psi should give 30% increase in $\dot{r}_a/\dot{r}_o$, which agrees reasonably well with the 25% measured.

An additional parameter becomes important when the pressure of accelerated PBAN propellants is increased beyond 1000 psi; local flooding of the surface by the metal oxide. This gives rise to globules with small r_s/a, which tends to reduce $\dot{r}_a/\dot{r}_o$. This agrees with the observation by Anderson and UTC. No theory is available, however, to predict the degree of flooding with pressure level.

Static burning rate. The analytic model clearly demonstrates the significance of static burning rate. Firstly, the experimentally observed trend of smaller $\dot{r}_a/\dot{r}_o$ of higher-burning-rate propellants is indicated. Secondly, $\dot{r}_a/\dot{r}_o$ depends inversely on the $\dot{r}_o$ to the first power but only on the

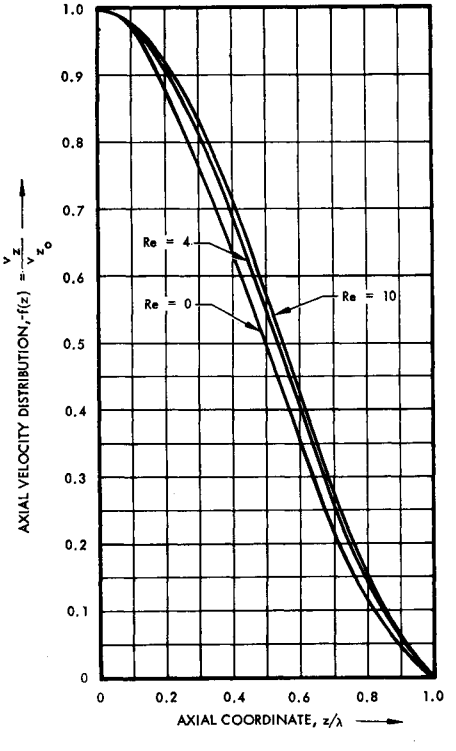

Fig. 7 Axial velocity distribution.

$\frac{1}{4}$ power of acceleration and pressure level. These effects are in accord with the experimental findings.

Metal content and powder size. The model developed here is not applicable to nonmetalized propellants. As previously mentioned models for the burning-rate augmentation of these propellants have been proposed by Sturm and Glick.

It is reasonable to expect that the metal content in the propellant will have a significant effect on globule size, and it is conceivable that the powder size of the metal will also influence the ultimate globule size. Unfortunately, no data are available to determine their effect. The adequacy of the model to predict the effect of metal content and powder size on burning-rate augmentation cannot be ascertained until more information is available concerning their influence on globule size.

An important feature of the model is its capability to predict an $\dot{r}_a/\dot{r}_o$ for accelerated propellants with refractory additives. The model predicts a small augmentation for the alumina propellant because the alumina melts and tends to form a layer which corresponds to a small r_s/a in Eq. (19). The tungsten, on the other hand, does not melt and the r_s/a term is larger. Thus a larger $\dot{r}_a/\dot{r}_o$ is predicted. This trend is substantiated by the data.

Burning time. The analysis of the model has not been extended to include transient effects. To do so requires an understanding of aluminum powder agglomeration and combustion to form an aluminum-oxide globule and the subsequent globule growth. The continual growth of an alumina globule, once it has formed, by aluminum particles which fall down the pit wall, collide, burn on its surface and leave a residue, gives rise to a monotonically increasing r_s, and decreasing r_s/a. This predicts a decreasing $\dot{r}_a/\dot{r}_o$ with time, which parallels Sturm's observations.

Conclusions

The photographic studies of the surface of a burning metalized composite propellant under acceleration show alumina globules retained by inertial forces in pits on the propellant surface. The observation that the pits persist leads to the conclusion that the presence of the globule augments the local propellant burning rate. Analysis indicates that the augmented burning rate is the result of conductive heat transfer from the particle, across the supporting gas flow, to the propellant surface. The capability of the analytic model to predict, where sufficient data are available, the observed trends in acceleration-produced burning-rate augmentation justifies confidence in the model's validity. The parameter for which the least information is available and trends are unpredictable is globule size. The ultimate assessment of the model's validity will only be possible after more data are available on globule formation and growth.

Appendix

Analysis of Flow between Particle and Propellant Surface

Discarding the higher-order terms of the Navier-Stokes equations for cylindrically symmetric flow between the particle and the surface, one obtains

$$(1/\eta)(\partial/\partial\eta)(\eta v_\eta) + \partial v_z/\partial z = 0 \tag{A1}$$

$$v_\eta(\partial v_\eta/\partial\eta) + v_z(\partial v_\eta/\partial_z) + \partial P/\partial\eta = (1/Re)\partial^2 v_\eta/\partial z^2 \tag{A2}$$

$$v_\eta(\partial v_z/\partial\eta) + v_z(\partial v_z/\partial z) + \partial P/\partial z = (1/Re)\partial^2 v_z/\partial z^2 \tag{A3}$$

where velocities and distances have been normalized with respect to the gas-efflux velocity at the propellant surface v_{z_o} and the particle-standoff distance. The Reynolds number is now defined as $Re = \rho_o v_{z_o}\lambda/\mu$.

It is reasonable to assume, in this problem, that the gas-efflux velocity is uniform under the particle which implies that v_z is independent of η, or $v_z = -f(z)$. Then the continuity equation requires

$$v_\eta = (\eta/2)f'(z) \tag{A4}$$

and radial momentum equation requires

$$P = (\eta^2/2)g(z) + h(z) \tag{A5}$$

Substituting these relationships into the axial momentum equation shows

$$g'(z) = 0 \quad \text{or} \quad g(z) = \text{const} = \delta/4 \tag{A6}$$

The radial momentum equation reduces to

$$f'^2 - 2ff'' + \delta = (2/Re)f''' \tag{A7}$$

With the boundary conditions, $f(0) = -1$, $f(1) = f'(0) = f'(1) = 0$. Assuming a solution of the form

$$f(z) = \sum_{i=0}^{5} a_i z_i \tag{A8}$$

leads to

$$f(z) = -1 + z^2\,\frac{[(3 - 2z) + Re(1 - z^2/2) + (Re^2/20)(5 - 2z^3)]}{1 + Re/2 + 3Re/20} \tag{A9}$$

which is plotted for various values of Reynolds number in Fig. 7. It is noted that $f(z)$ is not a strong function of Re in the range of interest and the $Re = 0$ curve can be used to estimate the others. Therefore

$$f(z) \simeq -1 + (3 - 2z)z^2 \tag{A10}$$

is sufficiently valid. The constant δ for the pressure distribution becomes

$$\delta = \frac{-24}{Re}\,\frac{1 + Re/2 + Re^2/6 + Re^3/24}{1 + Re/2 + 3Re^2/20} = \frac{-24}{Re}\,[F(Re)] \tag{A11}$$

There is no need to evaluate $h(z)$ in Eq. (A5), because only the pressure distribution along the particle surface is required.

The velocity distribution can now be used in conjunction with the energy equation to determine the heat transfer rate to the propellant surface. The significant terms in the energy equation are

$$v_z\partial h/\partial z = (1/Pe)\partial^2 h/\partial z^2 \tag{A12}$$

where h is the enthalpy per unit mass and Pe the Péclet number. The corresponding integral is

$$\frac{h - h_s}{h_p - h_s} = \frac{\int_0^z dy \exp\left[-\int_0^y Pef(w)dw\right]}{\int_0^1 dy \exp\left[-\int_0^y Pef(w)dw\right]} \tag{A13}$$

The integral of the velocity distribution function

$$\int_0^y f(w)dw = -y + y^3 - 0.5y^4 \tag{A14}$$

is close approximated by

$$\int_0^y f(w)dw \simeq -0.5 + 0.5(y - 1)^2 \tag{A15}$$

which is a more convenient expression for manipulation in the previous equation. Substitution of Eq. (A15) into Eq. (A13) and performance of the indicated operations yields the following expression for the enthalpy gradient at the propellant surface,

$$\left.\frac{\partial h}{\partial z}\right|_{z=0} = \left(\frac{h_p - h_s}{\lambda}\right)\left(\frac{2}{\pi}\right)^{1/2} Pe^{1/2}\,\frac{\exp(-Pe/2)}{\text{erf}\,(Pe/2)^{1/2}} \tag{A16}$$

This expression is used to determine the heat-transfer rate to the propellant surface.

References

[1] "Compilation of Rocket Spin Data," NASA CR 66641, July 1968, Emerson Electric and Space Division.

[2] Crump, J. E., "Aluminum Combustion in Composite Propellants," *Presented at the Second ICRPG Combustion Conference*, 1965.

[3] "Investigation of Performance Losses and Ballistic Effects in Solid Propellant Rockets (U)," UTC FR-2197, April 1967, United Technology Center.

[4] Glick, R. L., Hodge, B. K., and Caveny, L. H., "Effect of Acceleration on the Burning Rate of Composite Propellants," AIAA Paper 67-470, Washington, D.C., 1967.

[5] Northam, G. B., "On Experimental Investigation of the Effects of Acceleration on the Combustion Characteristics of an Aluminized Composite Solid Propellant," *Presented at the ICRPG/AIAA Solid Propulsion Conference*, Washington, D.C., July 19–21, 1966.

[6] Anderson, J. B. and Reichenbach, R. E., "An Investigation of the Effect of Acceleration on the Burning Rate of Composite Propellants," *AIAA Journal*, Vol. 6, No. 2, Feb. 1968, pp. 271–277.

[7] Horton, J. G., II, "Experimental Evaluation of Solid Propellant Rocket Motors under Acceleration Loads," *Journal of Spacecraft and Rockets*, Vol. 1, No. 6, Nov.–Dec. 1964, pp. 673–674.

[8] Northam, G. B. and Lucy, N. H., "On the Effects of Acceleration upon Solid Rocket Performance," *Journal of Spacecraft and Rockets*, Vol. 6, No. 4, April 1969, pp. 456–459.

[9] "Investigation of Internal Ballistic Effects in Spinning Solid Propellant Motors," UTC FR-2281, Oct. 1968, United Technology Center.

[10] Sturm, E. J. and R. E. Reichenbach, "An Experimental Study of the Burning Rates of Aluminized Composite Propellants in Acceleration Fields," AIAA Paper 68-529, Atlantic City, N.J., 1968.

APRIL 1971 J. SPACECRAFT VOL. 8, NO. 4

Development of a Fluidically Controlled Hydrazine Roll-Rate Control System

RICHARD W. SIEVERS*
Hamilton Standard, Division of United Aircraft Corporation, Windsor Locks, Conn.

AND

SAMUEL B. MARTIN†
Sandia Laboratories, Albuquerque, N. Mex.

A program was undertaken to design, develop, test and deliver three rocket engine modules (REM's) for flight feasibility testing on a re-entry test vehicle. These units, which provide positive/negative roll torques, consist of four hydrazine monopropellant engines, a propellant tank, pressurant tank, pressure regulator with pyrotechnic isolation, and a fluidically controlled propellant valve. Each REM, when coupled with a fluidic sensing and logic module, comprises a closed loop, fluidically controlled Roll-Rate Control System (RRCS) requiring no electrical power for operation. This paper describes the REM requirements, unique features and test results.

Introduction

IN April 1969 Sandia Laboratories contracted with Hamilton Standard, Division of United Aircraft Corporation, to design, test, fabricate and deliver three rocket engine modules (REM's) for flight feasibility testing. These REM's (Fig. 1), when coupled with fluidic sensing and logic modules developed by Sandia Laboraties, form self-contained, self-powered, closed-loop, roll-rate control systems (RRCS). These feasibility systems will be used to demonstrate, inflight, control of the resonant pitch-roll coupling phenomenon found in re-entry test vehicles. Roll-rate control torques are applied by two sets of hydrazine monopropellant rocket engines firing in pairs (Fig. 2). Except for the pyrotechnic system initiation, the RRCS is completely self-contained with sensing, logic and firing control of the engines accomplished fluidically without the use of electrical power. This approach provides system simplicity and reliability and reduces the system weight by eliminating the need for stored electrical power. Positive propellant expulsion is accomplished by the metallic diaphragm incorporated in the propellant tank. The over-all RRCS is packaged on a mounting frame and is designed to fit a limited envelope.

The program described in this paper was undertaken to provide flight feasibility hardware within a limited schedule. To minimize technical and schedule risks, conservative design margins where applicable, and proven components (by test or flight experience) were employed. An equally important consideration was the ability to ultimately incorporate, with minimum technical risk, the principal features of this system into a production unit.

The REM portion of the program was successfully concluded at Hamilton Standard with the completion of ground tests during which all major technical and performance objectives were met. The delivery of three flight REM's completed the program.

Presented as Paper 70-650 at the AIAA 6th Propulsion Joint Specialist Conference, San Diego, Calif., June 15–19, 1970; submitted June 26, 1970; revision received August 17, 1970. This work was supported by the U.S. Atomic Energy Commission. This paper describes the REM program which was conducted under Sandia Laboratories Contract 58-5782.

* Program Manager, Space Systems Department, Attitude Control Systems.

† Member Technical Staff.

System Requirements

The system design requirements were based on the needs of the ultimate flight production units; they allow for the